Supplementary Material: Rapid flipping of parametric phase states

Martin Frimmer,[1] Toni L. Heugel,[2] Žiga Nosan,[3] Felix Tebbenjohanns,[1] David Hälg,[3] Abdulkadir Akin,[3] Christian L. Degen,[3] Lukas Novotny,[1] R. Chitra,[2] Oded Zilberberg,[2] and Alexander Eichler[3,*]

[1]*Photonics Laboratory, ETH Zürich, CH-8093 Zürich, Switzerland.*[†]

[2]*Institute for Theoretical Physics, ETH Zürich, CH-8093 Zürich, Switzerland.*

[3]*Laboratory for Solid State Physics, ETH Zürich, CH-8093 Zürich, Switzerland.*

(Dated: Monday 25th November, 2019)

S1. EXPERIMENTAL DETAILS: OPTICAL TRAPPING SETUP

We implement the bitflip based on a deformation of the potential using an optically trapped nanoparticle [S1]. An extended sketch of the setup is shown in Fig. S1. In our experiment, we focus a linearly polarized laser beam (wavelength 1064 nm, focal power 80 mW) with a microscope objective (0.8NA) inside a vacuum chamber. A dielectric nanoparticle (silica, diameter 136 nm) is trapped by the optical gradient force in the laser focus. We collect the light scattered by the particle in the forward direction, where it interferes with the transmitted trapping beam, and send it to a standard four-quadrant detection scheme. We can therefore monitor the particle's motion along all three coordinate axes as a function of time. We call the optical axis the z direction, while the x and y axes lie in the focal plane with the x axis perpendicular to the polarization direction. The center-of-mass motion of the particle resembles three Duffing oscillators [S2]. Our experiments take place at 5×10^{-6} mbar, where the particle's motion is strongly underdamped. We use parametric feedback cooling to reduce the thermal oscillation amplitude of the particle along all three axes to 1 K [S3]. At these low oscillation amplitudes any non-linear mode coupling is negligible. The feedback signal is derived from the position measurement using a phase-locked loop whose output is frequency doubled and whose phase is adjusted to achieve cooling. This feedback signal is applied to an electro-optic modulator (EOM). Throughout this work, we focus on the x mode of the particle with natural frequency $f_0 \approx 164$ kHz.

Under parametric driving at a frequency $2f_d$ (with f_d close to the natural frequency f_0), the particle motion locks to the drive and acquires a large oscillation amplitude [S4]. Driving the x mode leaves the remaining degrees of freedom essentially

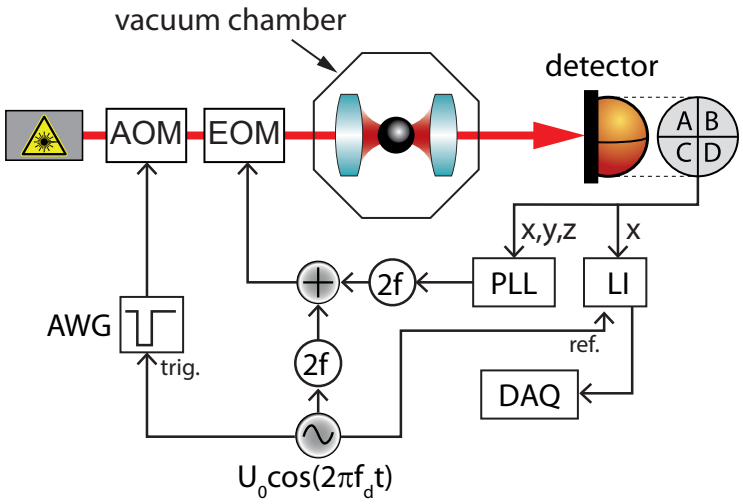

Figure S1: Experimental setup for phase flips via potential deformation.

*Electronic address: eichlera@phys.ethz.ch
†URL: http://www.photonics.ethz.ch

unaffected due to the large frequency difference between the modes ($f_z \approx 50$ kHz, $f_y \approx 130$ kHz). The parametric driving in our experimental system corresponds to a harmonic modulation of the laser intensity which sets the stiffness of the optical trap. We realize this parametric driving using the same EOM used for feedback cooling. The parametric driving signal is the frequency doubled output of a function generator producing a harmonic tone at f_d.

To effect the potential deformation leading to the flip of the parametron phase, we reduce the stiffness of the optical potential using an acousto-optic modulator (AOM). We have calibrated the device to switch the potential to half of the original stiffness by observing the natural frequency of the particle oscillation mode as a function of voltage applied to the AOM. To carry out a bitflip, we generate a square pulse of length τ_{def} with an arbitrary waveform generator (AWG). In order to effect the potential deformation at the desired time, we trigger the AWG by the parametric drive f_d to which the particle motion is locked in phase.

We extract the phase of the parametron by demodulating the detector signal of the measured particle position $x(t)$ at the drive frequency f_d using a lock-in amplifier (LI). The demodulated output of the LI is recorded by a data acquisition card (DAQ). A typical time trace of the phase output of the LI is shown in Fig. 2e of the main text. The timing resolution in this experiment is given by the bandwidth of the lock-in amplifier, which is chosen at 220 Hz in the presented experiments and is limited by the signal-to-noise ratio of the position measurement. With this timing resolution, the phase flips appear as essentially instantaneous in Fig. 2e and it is not possible to generate a highly time-resolved measurement of the phase as shown in Fig. 3e for the experiment with the LC resonator (which offers a dramatically higher signal-to-noise ratio). To gain information about the dynamics of the phase flip with higher timing resolution, we have devised the experiment shown in Fig. 2f. Here, our sub-microsecond control over the pulse length τ_{def} (provided by the waveform generator), allows us to investigate the dynamics of the phase flip on the timescale set by the natural frequency of the underlying resonator.

S2. MODEL FOR BIT-FLIP SUCCESS RATE

In this section, we describe the model giving rise to the solid line in Fig. 2f of the main text. Naively, one would expect P_{flip} to be a periodic rectangular function of τ_{def}, since the parametron will settle into the phase state $\phi = 0$ ($\phi = \pi$) if the deformation pulse takes it to a phase value in the range $[-\pi/2 \ldots \pi/2]$ ($[\pi/2 \ldots, 3\pi/2]$). However, Fig. 2(f) reveals that the transitions of $P_{\text{flip}}(\tau_{\text{def}})$ between zero and unity are not infinitely sharp but display a finite width of about 2 μs, which we attribute to thermomechanical fluctuations.

To model our system, we describe the phase-space distribution of the parametron as a thermally broadened coherent state with a Gaussian probability distribution. The width of this Gaussian is determined by the temperature of the nanoparticle's center-of-mass motion. Under feedback cooling, the root-mean squared amplitude due to thermal activation is around 2 nm. The displacement of the Gaussian from the origin by the coherent drive amounts to 7 nm. When the trapping potential is deformed to have natural frequency $f_0/2$, the phase-space distribution rotates around the origin at that frequency. We calculate the bit-flip success rate $P_{\text{flip}}(\tau_{\text{def}})$ as the fraction of the phase-space distribution falling into the halfspace with negative amplitude X, given that the system was started with its phase-space distribution initially centered on the positive X axis. The resulting (appropriately normalized) variation of the complementary error function is plotted in Fig. 2f as a solid line. We note that the width of the transitions from zero to unity is given by the ratio of the amplitude due to the thermal drive relative to the thermal population. Both these quantities were independently measured. The period of the undulations of P_{flip} is given by $f_0/2$, and a fixed parameter as well. The only free parameter we allow for is a phase shift corresponding to a temporal delay of 1.3 μs to account for the finite response time of our AOM switching the trapping potential.

S3. EXPERIMENTAL DETAILS: ELECTRICAL RESONATOR SETUP

In Fig. S2, we show the full electrical schematic of the experiment used for rapid phase flipping with the potential displacement method. Calibration measurements for this setup were performed in a previous study [S5]. A tuning voltage $U_{\text{tune}} \sim 2$ V is used to bring the diode into reverse bias, and a second (large) capacitance $C_1 = 47$ nF prevents DC currents from flowing withing the resonator.

For every flipping event, we first switch on the driving voltage U_{drive} to drive the resonator into parametric resonance and lock it to the drive. At the same time, the lock-in amplifier (HF2LI by Zurich Instruments) sends a clock signal phase-locked to U_{drive} to the FPGA. After waiting for the resonator to reach a steady state ($t_{\text{wait}} \geq 0.2$ s), we measure its phase state relative to the clock.

In the next step of the phase-flipping protocol, we use a RedPitaya FPGA to detect a zero-crossing of the clock signal. The FPGA then outputs a single rectangular pulse after a calibrated delay that depends on the measured resonator phase. This pulse triggers the lock-in amplifier to start logging U_{meas}, and is at the same time the 'force' applied to the resonator with an additional delay Δt (this delay ensures that the measurement captures the entire flipping process). We use an operational amplifier (THS4271D) to preserve a high quality factor of the resonator and to enable a rapid switch of U_{flip}. The measured resonator

response U_{meas} is measured as a time trace and later post-processed digitally in a computer. After the flipping event, the phase of the resonator is measured once more by the lock-in amplifier to verify a successful phase reversal.

For each phase flip event, we run the raw signal through a digital lock-in amplifier at f_d to obtain the phase space quadratures. We then perform a fast Fourier transform (FFT) and apply a SINC filter with a cut-off frequency at f_d to eliminate unwanted harmonic responses. After a back-transformation into the time domain, we calculate the phase ϕ that is shown in Fig. 3e.

S4. THEORY DETAILS: FOKKER-PLANCK SIMULATIONS OF RAPID FLIPPING

In the following, we numerically investigate the robustness of the switching protocol based on the potential-deformation method. In particular, we demonstrate that the flipping fidelity of the potential-deformation method is independent of the time when the switch is executed within the parametron oscillation cycle. We perform these investigations using numerical simulations of corresponding time-dependent Fokker-Planck equations [S6].

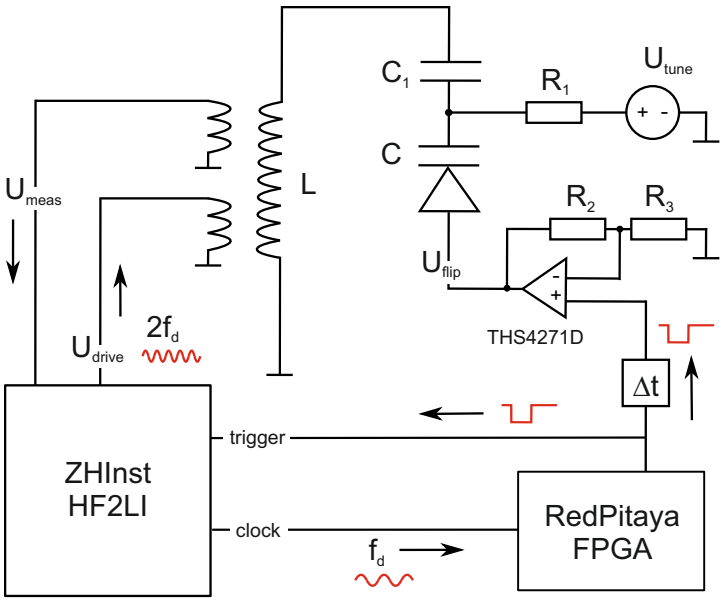

Figure S2: Experimental setup for phase flips via potential displacement.

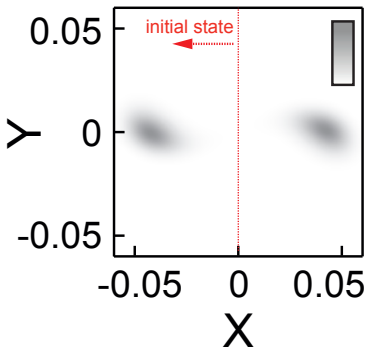

Figure S3: Probability density function (PDF) $p(X, Y, t)$ of the parametron's steady state for our simulation parameters. The colorbar ranges from $p = 0$ (white) to $p = 2425$ (grey). The integration of p over the entire phase space yields unity. We use the phase-space population in the half space $X < 0$ as the initial state for simulations of the bit-flip protocols.

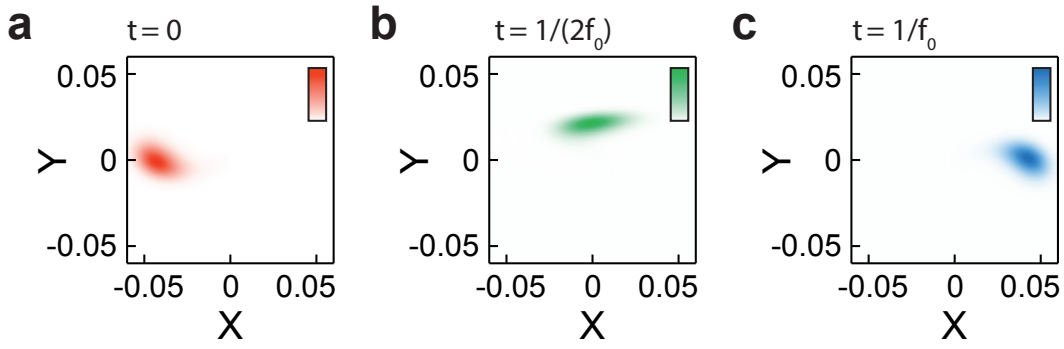

Figure S4: Fokker-Planck simulation of the potential-deformation protocol with noise. The bit-flip is initialized when the resonator has maximum (negative) displacement and minimum momentum. The three subfigures are snapshots of the flipping process at different times during the protocol and correspond to the three situations shown in Fig. 2d of the main text. The colorbars range from $p = 0$ (white) to $p = 4850$ (red/green/blue). (a) Initial state $p(X, Y, t = 0)$, corresponding to the steady state in Fig. S3 in the region $X < 0$ of phase space. (b) Probability density function (PDF) of the parametron in the middle of the flipping protocol, corresponding to time $t = 1/(2f_0)$. (c) PDF of the parametron at the end of the flipping protocol at time $t = 1/f_0$.

A. Details of the numerical model

In our analysis, we consider a nonlinear parametric resonator with additive force noise (originating, e.g., from thermal processes or from a noisy pulse). Our model can describe both experimental platforms used in this work (see [S5] and [S4]). We choose to discuss our model in the form of a mechanical resonator described by the equation of motion

$$\ddot{X} + \frac{\gamma}{m}\dot{X} + \omega_0^2\left[1 - \lambda\cos(2\omega_d t)\right]X + \frac{\alpha}{m}X^3 = \frac{F(t)}{m} + \frac{\sigma\xi(t)}{m}. \tag{S1}$$

Here, X is the displacement, $Y = \dot{X}$ the velocity, dots indicate differentiation with respect to time t, m is the effective mass, $\omega_0 = 2\pi f_0$ is the angular resonance frequency, $\gamma = m\omega_0/Q$ is a damping term, and α describes the strength of a cubic restoring force. The system is subject to a parametric drive with modulation depth λ at a rate $\omega_d = 2\pi f_d$. Deterministic external forces are summed up as $F(t)$. Stochastic forces are described by the noise intensity σ and the white noise process $\xi(t)$ with $\langle\xi(t)\rangle = 0$ and $\langle\xi(t)\xi(t')\rangle = \delta(t - t')$, where $\delta(t)$ is a Dirac-delta distribution.

The system can be described by the following Fokker-Planck equation for the probability density function (PDF) $p(X, Y, t)$ of finding the system at the phase-space point (X, Y) at time t. We rewrite Eq. (S1) as two coupled first order differential equations to obtain

$$\dot{X} = Y, \tag{S2}$$

$$\dot{Y} = \frac{1}{m}\left\{F(t) - \gamma Y - m\omega_0^2\left[1 - \lambda\cos(2\omega_d t)\right]X - \alpha X^3\right\} + \frac{\sigma}{m}\xi(t). \tag{S3}$$

The Fokker-Planck equation for $p(X, Y)$ is then given by [S6]

$$\begin{aligned}\frac{\partial}{\partial t}p(X,Y,t) = &- Y\frac{\partial}{\partial X}p(X,Y,t) - \frac{1}{m}\frac{\partial}{\partial Y}\left\{F(t) - \gamma Y - m\omega_0^2 X[1 - \lambda\cos(2\omega_d t)] - \alpha X^3\right\}p(X,Y,t) \\ &+ \frac{\sigma^2}{2m^2}\frac{\partial^2}{\partial Y^2}p(X,Y,t).\end{aligned} \tag{S4}$$

For all following calculations, we use the dimensionless parameters $m = 1$, $Q = 1000$, $\omega_0 = \omega_d = 1$, $\lambda = 0.003$, $\alpha = 1$, $F = 0$ and $\sigma = 2.4 \times 10^{-4}$.

In a first step, we find the steady-state probability distribution p_{steady} of the parametron, see false-color plot in Fig. S3. The distribution p_{steady} features appreciable values only in two distinct lobes in (X, Y) phase space. These two regions correspond to the two stable phase states of the parametron and differ in phase by π as expected. The width of the two lobes is given by the magnitude of the fluctuating forces σ together with the damping rate γ, while the radial distance of the lobes' respective centers from the phase-space origin is set by the driving strength λ and the non-linearity parameter α. In order to investigate the behavior of the phase-space distribution under our bit-flip protocols, we use as an initial distribution p_{ini} the part of p_{steady} residing in the half of phase space with $X < 0$. In other words, to obtain p_{ini}, we set p_{steady} to zero in the region $X > 0$ and renormalize the amplitude. In the following, we investigate the phase-space distribution $p(X, Y, t)$ after execution of a phase-flip protocol.

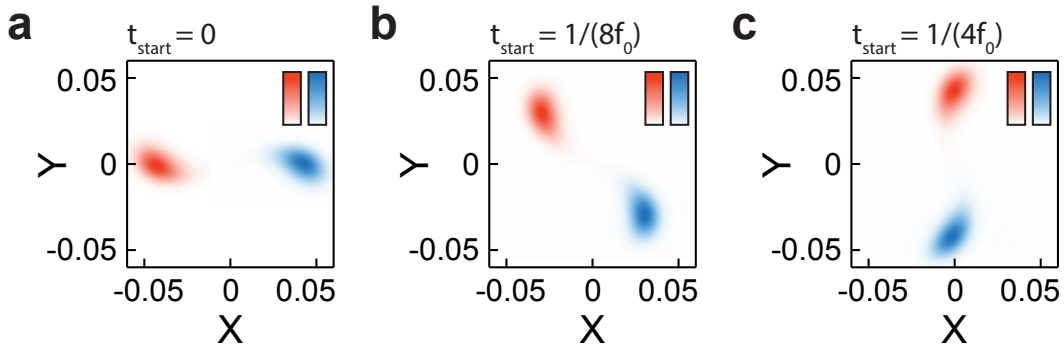

Figure S5: Fokker-Planck simulation of the potential deformation protocol with noise. The three subfigures correspond to flipping protocols that start at different times t_{start} within the oscillation cycle. The pulse length is set to the optimal value $\tau_{\text{def}} = 1/f_0$. Each panel combines the initial (red) and the final (blue) state in a single graph. (a) Potential deformation phase flip initialized at $t_{\text{start}} = 0$ when resonator has maximum displacement and minimum momentum. This is the same data as in Figs. S4a and c. (b) Potential deformation phase flip initialized at time $t_{\text{start}} = 1/(8f_0)$, when resonator has equal (normalized) displacement and momentum. (c) Potential deformation phase flip initialized at time $t_{\text{start}} = 1/(4f_0)$, when the resonator has minimum displacement and maximum momentum. The colorbars range from $p = 0$ (white) to $p = 4850$ (red/blue).

B. Numerical results: Potential deformation

We now numerically investigate the method termed 'potential deformation' introduced in the main text, where it was implemented with the levitated nanoparticle. To this end, starting with the distribution $p_{\text{ini}}(X, Y, t = 0)$, we switch the potential to $\omega_0 = 0.5$ during the flip time τ_{def}. In Fig. S4, we show the results of our simulations for an optimal pulse length $\tau_{\text{def}} = 1/f_0$. The time $t = 0$ where the pulse starts is chosen such that the resonator has maximum (negative) displacement and minimum momentum. (Note that this is the situation that we experimentally realized.) In the different panels, we show snapshots of $p(X, Y, t)$ at the beginning ($t = 0$, panel a), in the middle [$t = 1/(2f_0)$, panel b], and at the end ($t = 1/f_0 = \tau_{\text{def}}$, panel c) of the deformation pulse. We observe that the probability distribution is slightly distorted during the pulse (see panel b), However, at the end of the pulse, the phase-space distribution is essentially indistinguishable from the starting distribution, except that it has been rotated by π in phase space.

Having found that our phase-flip protocol based on potential deformation retains the shape of the initial phase-space distribution, we further investigate the robustness of our method to variations in the starting time of the pulse. In Fig. S5, we show the results of Fokker-Planck simulations of rapid phase flips for different starting times t_{start} of the potential-deformation pulse during the oscillation cycle of the parametron. In each panel, we show the starting distribution $p_{\text{ini}}(X, Y, t_{\text{start}})$ in red, together with the distribution $p_{\text{ini}}(X, Y, t_{\text{start}} + \tau_{\text{def}})$ in blue. Here, we have chosen the ideal pulse length $\tau_{\text{def}} = 1/f_0$. Note that Fig. S5a contains the combined information of Fig. S4a and c. Interestingly, looking at Fig. S5, we observe no appreciable difference in the resulting phase state as we vary the starting time of the pulse through the oscillation period of the parametron. These findings are in agreement with our expectation: During the time $\tau_{\text{def}} = 1/f_0$, which corresponds to half an oscillation period in the deformed potential, the phase state of the oscillator inverts, i.e., it evolves from (X, Y) to $-(X, Y)$, irrespective of the starting state. Accordingly, our bit-flip protocol based on potential deformation can be executed at any arbitrary point in time throughout the parametron oscillation cycle. Furthermore, our results show that the phase-flip protocol based on potential deformation leaves the width of the phase-space distribution essentially unchanged. Consequently, we conclude that the protocol is robust against inevitable additive force noise which can arise due to coupling to a thermal bath.

[S1] J. Gieseler, B. Deutsch, R. Quidant, and L. Novotny, Phys. Rev. Lett. **109**, 103603 (2012).
[S2] J. Gieseler, L. Novotny, and R. Quidant, Nature Physics **9** (2013).
[S3] V. Jain, J. Gieseler, C. Moritz, C. Dellago, R. Quidant, and L. Novotny, Phys. Rev. Lett. **116**, 243601 (2016).
[S4] J. Gieseler, R. Quidant, C. Dellago, and L. Novotny, Nature Nanotechnology **9**, 358 (2014).
[S5] Z. Nosan, P. Märki, N. Hauff, C. Knaut, and A. Eichler, Phys. Rev. E **99**, 062205 (2019).
[S6] C. Gardiner, *Stochastic Methods*, Springer-Verlag Berlin Heidelberg (2009).